

EXPERIMENTAL AND COMPUTATIONAL STUDY OF TWO FLAPPED AIRFOILS AT LOW REYNOLDS NUMBERS

Nea Ylilammi*, André Valdetaro Gomes Cavalieri**, Erkki Soinne*

*Aerodynamics Research Group, Aalto University School of Science and Technology, Finland, nea.ylilammi@tkk.fi **Aeronáutica e Mecânica, Instituto Tecnológico de Aeronáutica, Brazil

Keywords: *airfoil, CFD, experiment, low Reynolds number*

Abstract

In this work, two different airfoils, NACA 2412 and SD 7062, with plain flaps, were tested experimentally at a low Reynolds number range typical for Unmanned Aerial Vehicles. The measured results were then compared with a handbook method presented by Roskam and CFD codes, XFOIL, and FINFLO. The purpose of this work was to study the effect of low Reynolds number and flaps, as well as the capability of the studied methods to predict these effects.

1 Introduction

During the past three decades the interest in unmanned aerial vehicles (UAVs) has increased due to their suitability for many mission types. UAVs have been used in missions related to surveillance and ship decoys as well as detection of electrical, chemical, nuclear and biological materials. These mission types require the UAVs to fly at low velocities with long endurance. According to Mueller and DeLaurier (2003), the UAVs are required to fly at altitudes between 3 to 300 meters with flight speeds of 20 to 100 km/h. The wing spans of these vehicles are less than 6 meters.

The requirements set the UAVs to fly within a low chord Reynolds number range, varying from approximately 15,000 to 500,000. A number of differences occur in the flow properties in this velocity range. These are the presence of hysteresis in the aerodynamic curves, the non-linearity in the lift curve and the different location of transition from laminar to turbulent flow that are mainly caused by laminar separation bubbles and laminar separation as

discussed by Carmichael (1981) and Selig et al (1996).

Although a number of studies exist about the problems related to this flow velocity range, not much aerodynamic data exists for wing sections with high-lift devices or control surfaces. Therefore in this work, the aerodynamic parameters of two flapped airfoils, NACA 2412 and Selig SD 7062 were measured with flap deflections ranging from 0 to 30 degrees. The tests were performed within a dynamic pressure range typical for future small UAVs. Furthermore, suitable computational methods were studied.

2 Experimental procedures

The wind tunnel experiments of this work were performed in the Laboratory of Aerodynamics, Propulsion and Aeronautical Systems of Instituto Tecnológico de Aeronáutica, ITA, in Brazil. The used wind tunnel, displayed in Figure 1, was open circuit type capable to produce dynamic pressures between 9,8 to 509,9 Pa. The flow velocity range of the tunnel varies from 4 to 30 m/s and the turbulence intensity is 0,5% at the highest velocity.

The force measurements were performed with a triangular balance plate. A Pitot tube was used in the measurements of the static and dynamic pressures. The angle of attack was changed manually with a rotating device fixed to the model's metal axis. It allowed the angle of attack to be varied by every one degree for 360 degrees with an accuracy of ± 0.5 degrees.

For the Selig SD 7062 experiments, end plates were used on both sides of the model in order to minimize the three-dimensional effects.

The purpose of the end plates was to separate the boundary layer of the wind tunnel walls from the two-dimensional model. The used end plates were similar to those in the measurements performed by Girardi et al. (2007).

The tested NACA 2412 airfoil, shown in Figure 2, had a plain flap of 30 % of the airfoil's chord length. The flap was attached to the main airfoil with 8 metal hinges creating an open gap of 2 mm, 58% of which was sealed in the spanwise direction by the hinges. The metal axis used to connect the model to the experimental apparatus was at the quarter-chord of both of the tested airfoils.

The used SD 7062 airfoil had a plain flap of 20 % of the airfoil's chord length, which was attached to the main airfoil with metal hinges. A gap of 4 mm was sealed with thin tape on both sides of the airfoil. The span of the model was 418 mm, leaving approximately a 1.25 mm gap between the end plates and the model. A picture of the SD 7062 model is shown in Figure 3.

For the measurements of the hinge moment of the SD 7062 model, a particular apparatus was built into the lower surface of the model. The measurements were performed with a load cell capable of measuring forces up to 1 kgf and which was located inside the model.

A calibration was performed to all the four load cells as well as the anemometric system in order to define the correlation between the voltage read by the acquisition system and the experienced forces and pressures. The calibration procedure for the load cells was performed with a set of standard masses and a system of pulleys and wires.

The calibration was done with 20 loads, which increased incrementally from zero to the maximum value estimated for the load cell in question, and then down to zero again. During a sampling time of one second, 1000 measurements were performed. The average value of these measurements was then correlated with the imposed force. The calibration of the anemometric system was performed with the same idea.

For both wing sections the experiments were performed at 5 velocities within the achievable dynamic pressure range. For NACA 2412 the measured Reynolds numbers were

260000, 210000, 120000, 92000 and 61000. For Selig SD 7062, the corresponding values were 420000, 320000, 250000, 150000 and 84000. The used flap deflections varied from $\delta_f = 0$ to 30 degrees.

For the flap angle alignments of both airfoils, the inaccuracies were estimated to be ± 0.5 degrees. Since early studies on the SD 7062 model showed a small deflection of the flap under the influence of aerodynamic forces, the overall accuracy of the flap angle is estimated to be ± 1 degree for this model.

The measurement accuracy was estimated with the help of the calibration procedure during which the data acquisition system calculated the standard deviation for each sensor. Based on these calculations the uncertainties for the aerodynamic coefficients were estimated by the methods given in reference [3].

For NACA 2412 experiments, the achieved accuracies are ± 0.037 for the lift coefficient and ± 0.012 for the pitching moment coefficient. For the drag coefficient the accuracy is ± 0.007 . For the SD 7062 measurements, the calculated accuracy for the lift coefficient is ± 0.032 and ± 0.01 for the pitching moment coefficient. For the drag coefficient the calculated accuracy is ± 0.009 and for the hinge moment coefficient it is ± 0.005 .

The influence of the wind tunnel walls was corrected for the lift and pitching moment coefficients by using a Matlab code written by Gomes (2007). This corrective method uses potential flow calculations, thus these results are somewhat approximate for flows with separation.

3 Computational methods

3.1 Handbook method

The calculation method given in Roskam (2000) is based on statistical data that is mostly taken from USAF Stability and Control Datcom (1978). The handbook method is fairly accurate for higher Reynolds numbers and was therefore chosen to be a part of this study. As the experimental data was compared with the handbook results, the need for corrective

calculation technique for lower Reynolds number could be studied.

3.2 XFOIL

XFOIL is a panel method code with boundary layer corrections that is developed by Mark Drela (1989). The different airfoil geometries used in the XFOIL analysis were created with XFOIL from the basic coordinates of the unflapped airfoils. For NACA 2412 these were taken from the XFOIL database and for Selig SD 7062 from Selig et al. (1997). The calculations were performed by assuming that the wind tunnel was in normal conditions, and hence the inserted transition instability parameter N_{crit} was set to the value of 9. For all the calculated cases convergence was reached in 200 iteration cycles within an accuracy range of 1 %.

3.3 FINFLO

The Reynolds-averaged Navier-Stokes solver, FINFLO, has been developed since 1987 at the Helsinki University of Technology. The flapped geometries used in FINFLO were taken from the XFOIL analysis. As FINFLO requires a grid around the studied airfoil geometry, a Gridgen generated mesh was individually developed for all the studied cases. An example of a generated grid is shown in Figure 4.

The mesh consisted of 480 x 192 cells in all of the computed cases. As explained in Soenne (1998), in order to guarantee sufficient computational accuracy in the boundary layer, the dimensionless normal distance from the airfoil surface at the first cell center, y^+ , should not exceed the value of 1. As the used first cell height was less than $4,61 \cdot 10^{-5} h/c$ in all of the simulated cases, the required accuracy was fulfilled in the mesh generation.

The cell sizes were varied along the airfoil surface by using the hyperbolic tangent function implemented in the grid generation software, Gridgen. In the chordwise direction, the ratio of the sizes between two consecutive cells remained less than 1.1 inside the boundary layer and about 1.4 at the outer edges of the mesh. In the normal direction, the cell sizes remained constant inside the boundary layer.

Stretching was successively applied only far from the boundary layer and remained less than 1.4 in the outer edges. The sufficient amount of iteration cycles was examined to be 1000 with the desired accuracy of 2% in all aerodynamic coefficients.

The used turbulence model in the calculation was a $k-\omega$ model, developed by Hellsten (2004). The model was applied with high-Reynolds number explicit algebraic Reynolds-stress model (EARSM) utilizing linear Wallin-Johansson (WJ) pressure-strain model. As the FINFLO calculation procedure requires a manual input for the transition location, the results given by XFOIL were applied. During the calculation, this location remained fixed since the code itself does not perform any iteration of the transition location.

4 Result Analysis

4.1 Experimental Results

In Figure 5, the NACA 2412 results for the lift coefficients with zero flap deflection are shown. It can be seen that the stall angle and the maximum lift coefficient are somewhat reduced at the lower flow velocities. In addition, there seems to be a slight decrease in the linear part length of the lift curves at the lower Reynolds numbers. These effects are caused by an increase in the boundary layer thickness as the flow velocity is reduced. The thicker boundary layer decreases the effective camber of the airfoil which results in a decrease in the lift force. This viscosity effect increases with the angle of attack.

Another observation can be done for the nonlinearity of the lift curves in the medium range of the angles of attack. The nonlinearity becomes more severe as the flap deflection increases. This can be seen in Figure 6, where the results for flap angle of 20 degrees are shown. There is a rapid increase of the lift curve slope at the vicinity of the zero angle of attack. The lift curve slope then reduces as the angle of attack is increased.

This is probably caused by laminar separation that turns into a separation bubble as

the separated boundary layer transits into a turbulent one and reattaches itself to the airfoil surface. This separation increases the boundary layer thickness on the upper surface of the airfoil. On the lower surface of the airfoil, the boundary layer thickness reduces. This effect increases as the angle of attack gets higher. The increase in the effective camber of the airfoil is also indicated by the change in the pitching moment curves that can be observed around the zero angle of attack. In addition, the changes of the position and the size of the laminar separation bubble (LSB) contribute to the non-linearities of the lift curves.

The reduction in the lift gradient and growth in the pitching moment curves as the angle of attack is furthermore increased, are on the contrary caused by a decrease in the effective camber, which may be explained by the total effects of the laminar separation bubble. The effects can also be seen in the NACA 2412 pitching moment curves of which an example is presented in Figure 7 at flap angle of 0 degrees.

The moment coefficients measured at the highest Reynolds number are comparable to the ones measured by Abbott and Von Doenhoff (1949). However, the effect of the lower flow velocities is seen as an increase in the absolute value of the pitching moment. The earlier stall experienced at the lower Reynolds numbers causes the moment curve to decrease at smaller angles of attack. Another observation is that as the Reynolds number is decreased, the stall becomes more abrupt.

In Figure 8, the drag polar curves for studied Reynolds numbers at 0 flap deflection are presented. Also the results by Abbott and Von Doenhoff (1949) and the measurements given in Althaus (1980) are included for comparison.

In the velocity range of interest, the drag is known to increase with decreasing Reynolds number. This is caused by the laminar separation along the airfoil surface that modifies the pressure distribution on the surface and the thickness of the boundary layer on both upper and lower surfaces of the airfoil. Another cause is the increase in the friction coefficient both for

laminar and turbulent boundary layers as the flow velocity is decreased.

Although the measured drag polars seem to support this fact, a noticeable difference can be seen between the present experimental results and the ones presented by Althaus (1980) in the lift coefficient range from 0 to 1. This difference between the drag results can be explained with the dissimilarity of the used models. In the current tests, the used airfoil had a plain flap of 30% of the chord. On the contrary, the wing section used by Althaus (1980) did not have a flap. Consequently, the current NACA 2412 airfoil had a gap between the main airfoil and the flap that may have caused the observed drag increase.

This conclusion is supported by ESDU (1992), where the estimated drag increase due to a gap between a main airfoil and a plain flap is given as a function of CL. According to ESDU, the drag coefficient increase varies linearly from 0.014 to 0.026 in the CL range from 0 to 0.6. Similar experimental results were achieved for the SD 7062 airfoil.

4.2 Handbook method results

In Figures 9, 11 and 12, the experimental results are compared with the ones predicted by the calculation method presented in Roskam (2000). The aerodynamic properties studied for both NACA 2412 and SD 7062 wing sections were the lift curve slope and the lift and pitching moment increments due to flap deflection. For the latter airfoil, also the hinge moment increments were analyzed.

In Figure 9, the experimental lift curve slopes of the SD 7062 airfoil are presented together with the values measured by Selig et al. (1997). The values predicted by the handbook method, which are fairly accurate for higher Reynolds numbers, are up to 15 % higher than the ones collected experimentally.

Also, there is a decrease in the lift curve slopes as the Reynolds number is reduced. This is probably caused by the increase in the boundary layer thickness with decreasing velocity, which in turn decreases the effective camber of the airfoil. This viscosity effect increases with angle of attack and hence the lift

curve slopes within the studied Reynolds number range are reduced.

The measured lift curve slopes of the NACA 2412 and the SD 7062 airfoils are plotted in Figure 10. The curves seem to behave in a similar manner with decreasing Reynolds number. Also noticeable is that the measured lift curve slopes of the studied airfoils tend to settle to the same values along their common Reynolds number range. This is an interesting result, since the airfoils studied in the current work have very different backgrounds in their development as well as usage. However, more experimental data needs to be collected to establish a general trend for these lower Reynolds numbers. Nevertheless, the found similarity can be used as a starting point in the analysis of airfoils for these flow velocities.

In Figure 11, the lift increments due to flap deflection of the SD 7062 airfoil are presented. As can be observed, the experimental results are lower than the ones given by the handbook method, especially as the flap deflection increases. The accuracy of the handbook method deteriorates at low Reynolds numbers.

In order to develop a precise calculation method that could be used for reliable predictive design of all kinds of wing sections, a large amount of airfoil data needs to be collected and combined. However, with the results gathered from the performed measurements in this work, corrective curves were created that can be used as a guidance in the preliminary analysis of UAVs' wing sections with ailerons or flaps.

This was done by first developing trendlines of the measured lift increment curves with a careful analysis of the results. Corrective curves were then developed from the trendlines by dividing them with the lift increment values calculated with the handbook method.

For the SD 7062 wing section, there was no consistent or major variation along the flow velocity range tested. Therefore, an average curve from the results was created that predicts the behavior of the lift increments with sufficient accuracy. This average corrective curve is presented in Figure 12. Similar analysis, not shown in here, was done for the NACA 2412 lift increments and also for the pitching moment increments of both airfoils.

The hinge moment increments of the Selig SD 7062 airfoil are studied in Figure 13. Since the values calculated with the handbook method seem to fit fairly well with the experimental results, no correction technique is needed for the hinge moment increments. The used measuring equipment for the hinge moment properties probably caused some flow disturbance on the lower surface of the airfoil. This may have caused some of the discovered differences between the calculated and measured values.

4.3 XFOIL results

The results for the lift curve slope of the SD 7062 wing section are presented in Figure 9. This method shows a reduction in lift curve slope with decreasing Reynolds number, but the values differ 0 - 13% from the measurements.

The lift increments calculated with XFOIL for the SD 7062 wing section are given in Figure 14. The calculations performed with XFOIL underpredicted the lift increments whereas the handbook method gave only one curve without Reynolds number effect overpredicting the increments. Although some differences arise between XFOIL and experimental results, XFOIL shows promising potential in predicting lift increment effects at the low Reynolds number regime in question with the exception of $Re = 84000$.

The hinge moment measurements of the SD 7062 airfoil were also compared with the predictions of XFOIL, see Figure 15. The calculated hinge moment increments are lower than the ones gathered experimentally and the difference increases with increasing flap deflection. Overall, the values given by the handbook method were more accurate.

One reason for the difference between the measured hinge moments and the XFOIL results can be the slight difference in the airfoil geometries. By using the geometry creation method implemented in XFOIL, the gap area, which was sealed with a tape on the tested model, could not be generated exactly.

4.4 FINFLO results

Finally the measured lift and pitching moment increments were compared with the results

calculated with FINFLO. For the SD 7062 airfoil, the lift increment comparison is presented in Figure 16. The corresponding results of the SD 7062 pitching moment increments are shown in Figure 17. The corresponding results for the NACA 2412, not shown here, behaved in a similar manner.

The comparison of the SD 7062 results shows fairly similar behavior as was seen in the previously presented results by XFOIL. As for the XFOIL calculations, the FINFLO predictions of the flap efficiency are lower than experimentally measured and this difference grows as the flap deflection increases. On the pitching moment increments, the computed results are fairly accurate in comparison with the experimentally collected values.

5 Conclusions

Two airfoils, NACA 2412 and SD 7062, with plain flaps were examined experimentally and with three different computational methods. Emphasis was given to the efficiency of flaps in a critically low Reynolds number range typical for UAVs. As the predictions given by the handbook method presented by Roskam (2000) were expectedly too high for the low Reynolds number range, the need for corrective curves was acknowledged.

The results calculated with the XFOIL code gave fairly accurate results for the Reynolds number regime of interest. However, the efficiency of the flaps was found to be underestimated. Corresponding accuracy was achieved with FINFLO CFD code. On the other hand, FINFLO is not capable to compute aerodynamics of a priori given airfoil as it lacks a transition routine. This is a shortcoming when studying low number airfoils. Furthermore, this method requires a considerable amount of computer time.

Acknowledgements

The authors are grateful for the staff of the laboratory of Prof. Kwei Lien Feng, Instituto Tecnológico de Aeronáutica, in Brazil.

References

- [1] Abbott I.H. and von Doenhoff A.E., *Theory of Wing Sections: Including a Summary of Airfoil Data*, McGraw-Hill, New York, 1949.
- [2] Althaus D., *Profilpolaren fuer den Modellflug*, Neckar-Verlag, Vs-Villingen, Germany, 1980.
- [3] Assessment of Experimental Uncertainty with Application to Wind Tunnel Testing, A Standard, AIAA S-017A, 92 p., 1999.
- [4] Carmichael B.H., Low Reynolds number airfoil survey. Vol. 1, NASA CR 165803, 105 p., 1981.
- [5] Drag due to gaps round undeflected trailing-edge controls and flaps at subsonic speeds, ESDU, Engineering Sciences Data Unit, Item No. 92039, 12 p., November 1992.
- [6] Drela M., XFOIL: An Analysis and Design System for Low Reynolds Number Airfoils, *Conference on Low Reynolds Number Airfoil Aerodynamics*, University of Notre Dame, pp. 1-12, June 1989.
- [7] Girardi R.M., Cavalieri A.V.G. and Araújo T.B., Experimental Determination of the Wing Airfoil Aerodynamic Characteristics and Flap Hinge Moment of the Wing Airfoil used at ITA's Unmanned Aerial Vehicle (UAV), *19th International Congress of Mechanical Engineering*, Brasília, 10 p., Nov 5-9, 2007.
- [8] Gomes C.D.A.N., Cavalieri A.V.G., Girardi R.M. and Araújo T.B., Correction of Wind Tunnel Results for the Airfoils of ITA's Unmanned Aerial Vehicle, *19th International Congress of Mechanical Engineering*, Brasília, 9 p., Nov. 5-9, 2007.
- [9] Hellsten A., New Two-Equation Turbulence Model for Aerodynamics Applications, TKK-DISS-1827, 191 p., 2004.
- [10] Mueller T.J. and DeLaurier, J.D., Aerodynamics of Small Vehicles, *Annual Review of Fluid Mechanics*, pp. 89-111, 2003.
- [11] Newcome L.R., *Unmanned aviation: a brief history of unmanned aerial vehicles*, American Institute of Aeronautics and Astronautics. Reston, VA, 2004.
- [12] Roskam J., *Airplane Design Part VI: Preliminary Calculation of Aerodynamic, Thrust and Power Characteristics*, DARCorporation, pp. 215-244, 280-310, 2000.
- [13] Selig M.S., Guglielmo J.J., Broeren A.P. and Giguere P., Experiments on airfoils at low Reynolds numbers, AIAA, *Aerospace Sciences Meeting and Exhibit*, Reno, NV, Jan.15-18, pp 1-8, 1996.
- [14] Selig M.S., Lyon C.A., Broeren, A.P., Giguere, P. and Gopalarathnam, A., *Summary of Low-Speed Airfoil Data – Vol. 3*, SoarTech Publications, Virginia Beach, 1997.
- [15] Soinne E., Validation of CFD Computations on Control Surfaces, KTH Department of Aeronautics Report 98-15, Royal Institute of Technology, Stockholm, Sweden, 83 p, 1998.

EXPERIMENTAL AND COMPUTATIONAL STUDY OF TWO FLAPPED AIRFOILS AT LOW REYNOLDS NUMBERS

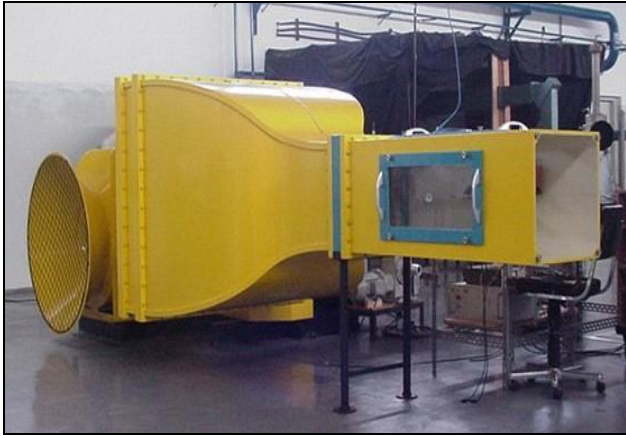


Fig. 1. ITA's open jet wind tunnel.

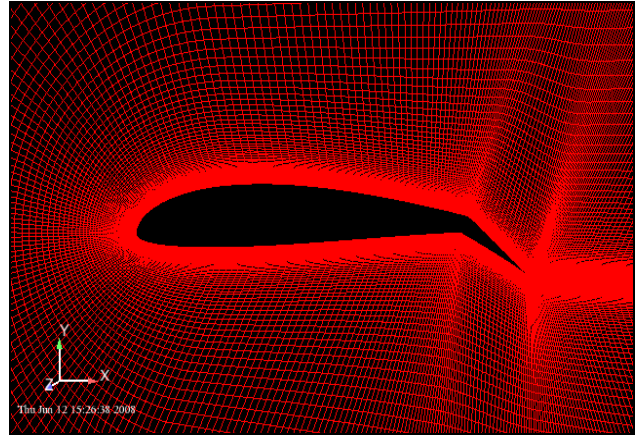


Fig. 4. Used mesh over the Selig SD 7062 airfoil at the flap angle of 30 degrees.

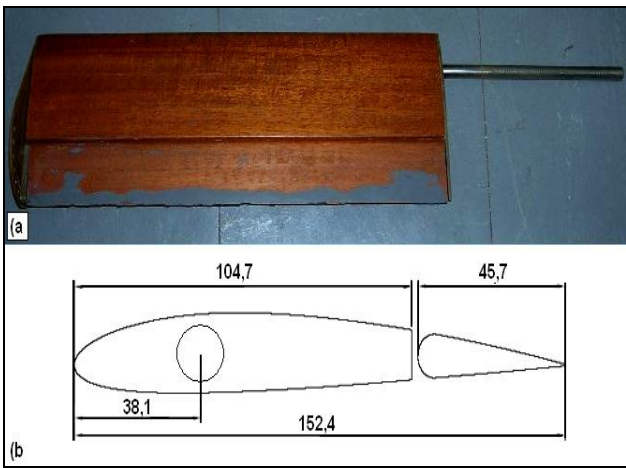


Fig. 2. (a) The tested NACA 2412 model and (b) its geometry in mm.

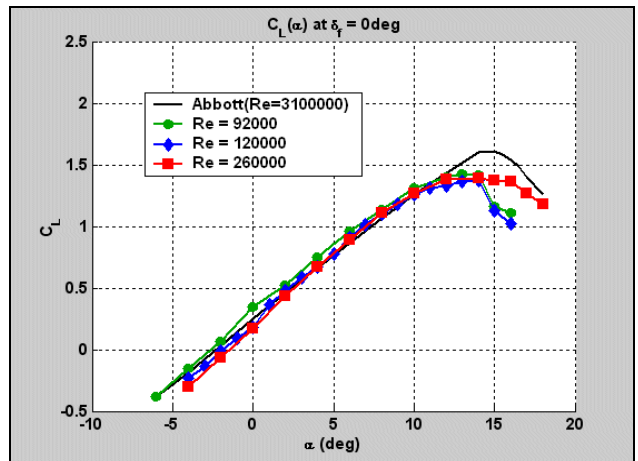


Fig. 5. Experimental lift coefficient curves of NACA 2412 at zero flap deflection together with the results given in Abbott and Von Doenhoff (1949).

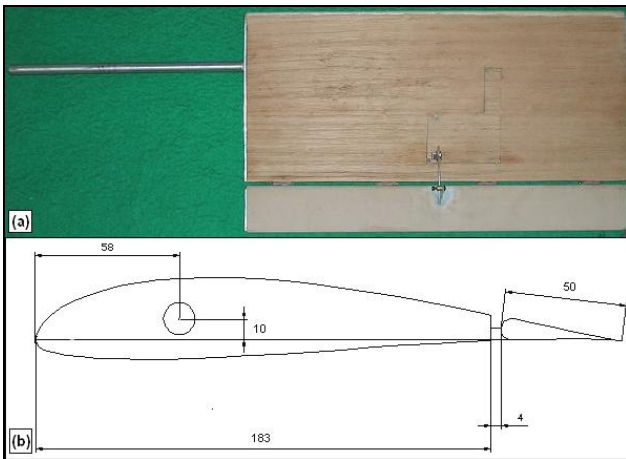


Fig. 3. (a) The tested Selig SD 7062 model and (b) its geometry in mm.

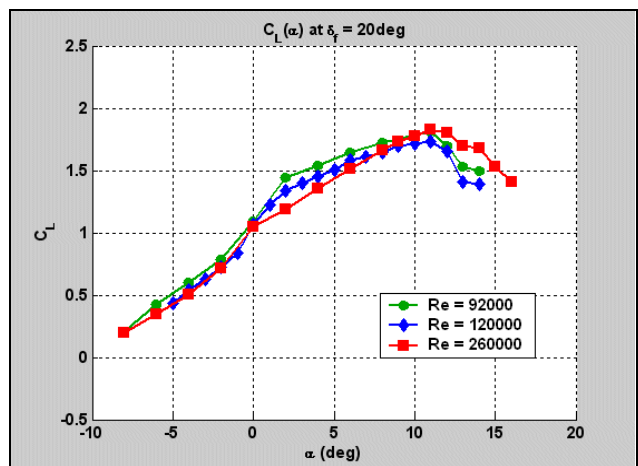


Fig. 6. Experimental lift coefficient curves of NACA 2412 at flap deflection of 20 degrees.

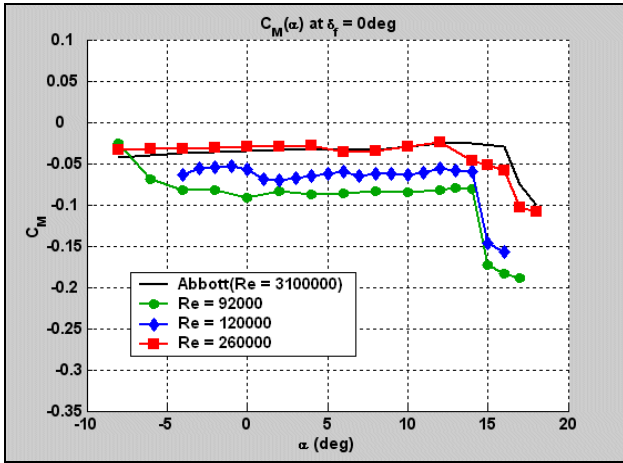


Fig. 7. Experimental moment coefficient curves of NACA 2412 at zero flap deflection together with the results given in Abbott and Von Doenhoff (1949).

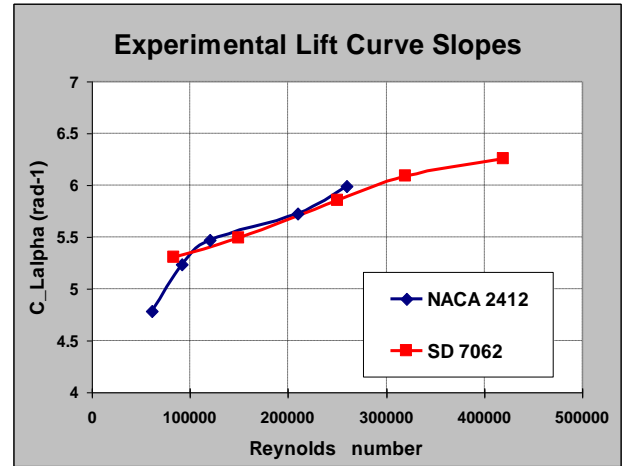


Fig. 10. Measured lift curve slopes of unflapped NACA 2412 and SD 7962 airfoils.

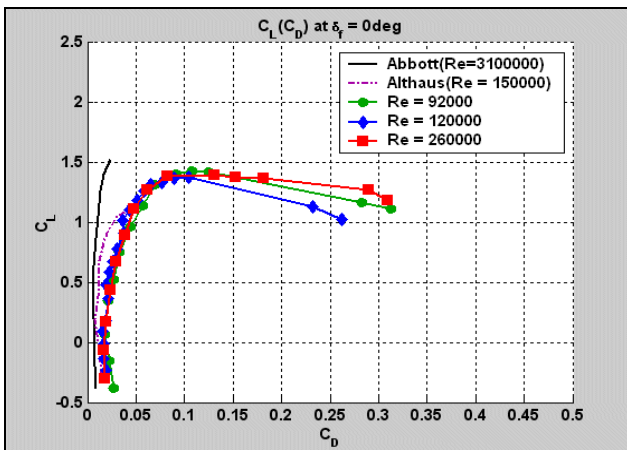


Fig. 8. Experimental drag polar curves of NACA 2412 at zero flap deflection together with the results by Abbott and Von Doenhoff (1949) and Althaus (1980).

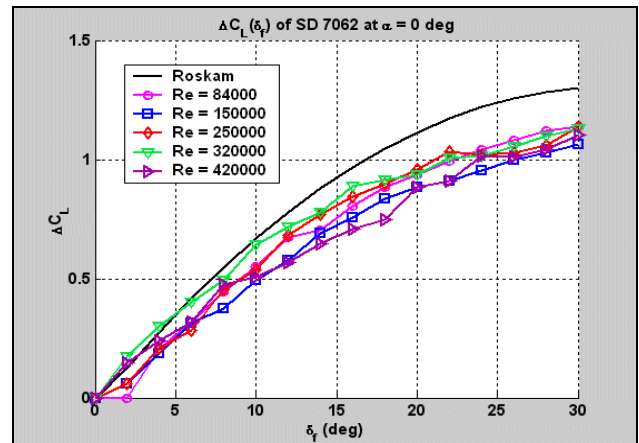


Fig. 11. Comparison of the measured SD 7062 lift increments at zero angle of attack with the ones calculated with the handbook method.

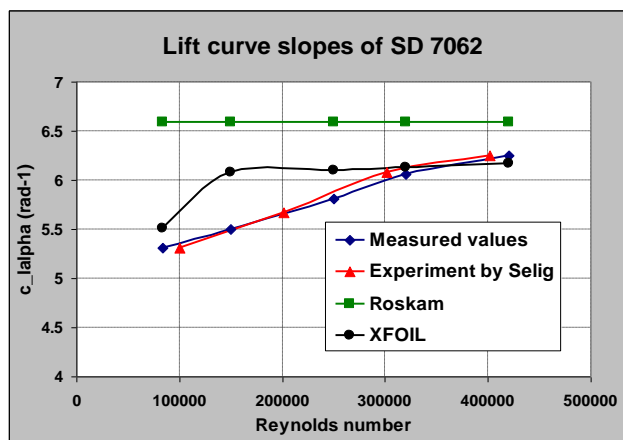


Fig. 9. Comparison of the measured SD 7062 lift curve slopes with the ones calculated with the method in Roskam (2000) at zero flap deflection and angle of attack.

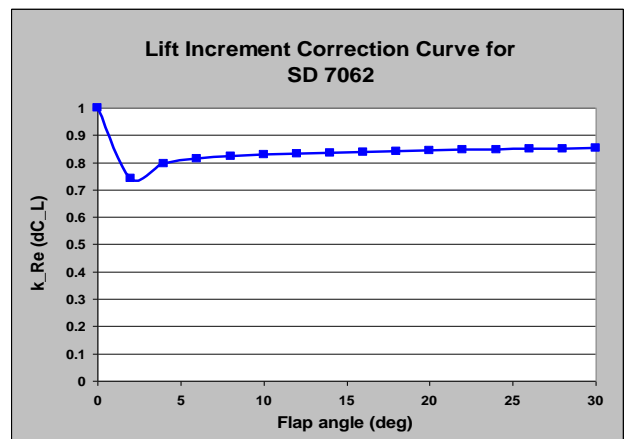


Fig. 12. Lift increment correction curve for the SD 7062 airfoil.

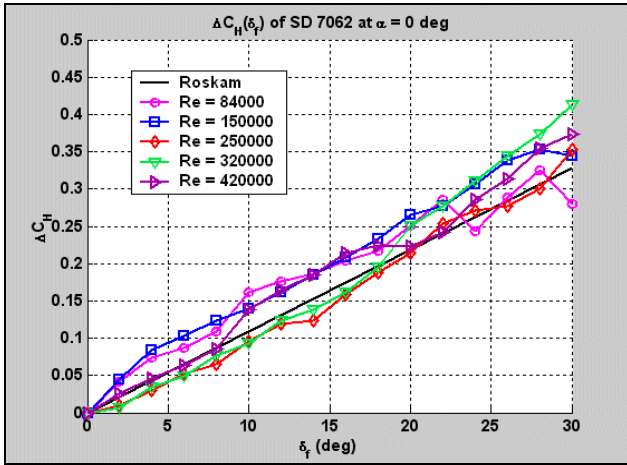


Fig. 13. Comparison of the measured SD 7062 hinge moment increments at zero angle of attack with the ones calculated with the method presented in Roskam (2000).

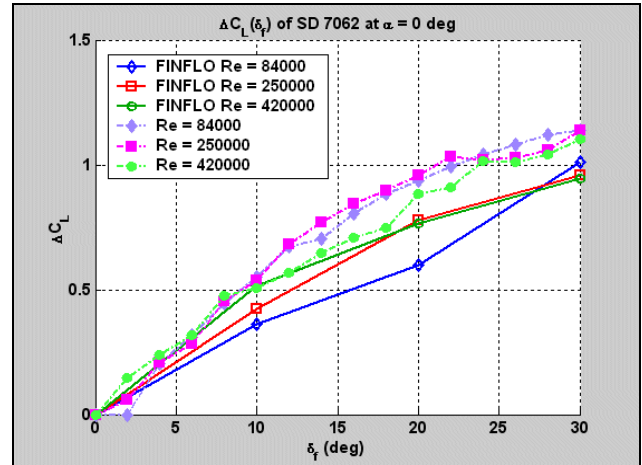


Fig. 16. Comparison of the measured SD 7062 lift increments at zero angle of attack with the ones calculated with FINFLO.

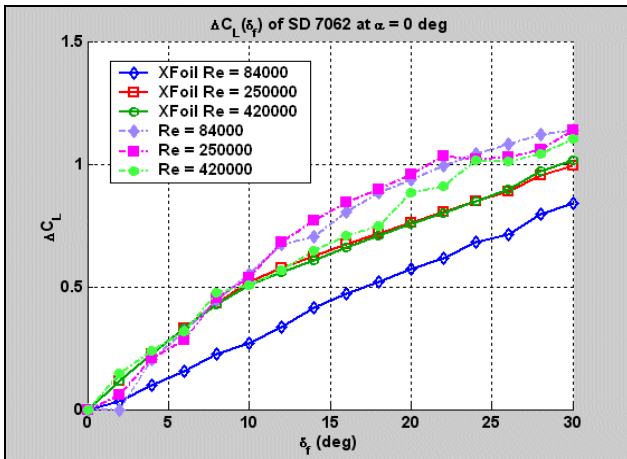


Fig. 14. Comparison of the measured SD 7062 lift increments at zero angle of attack with the ones calculated with XFOIL.

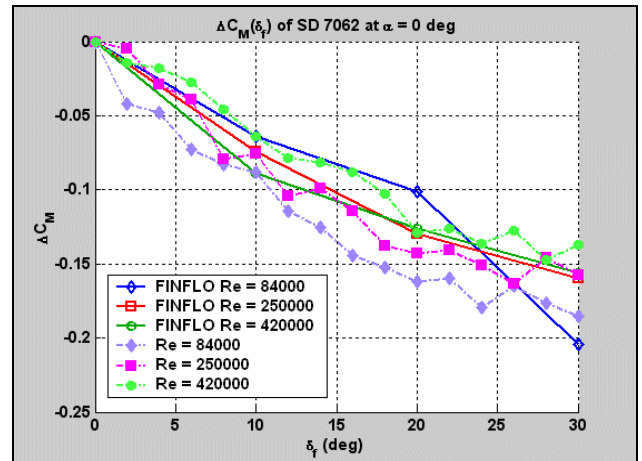


Fig. 17. Comparison of the measured SD 7062 pitching moment increments at zero angle of attack with the ones calculated with FINFLO.

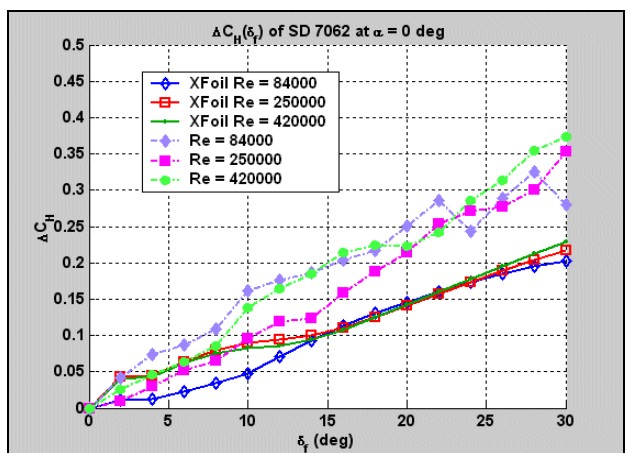


Fig. 15. Comparison of the measured SD 7062 hinge moment increments at zero angle of attack with the ones calculated with XFOIL.

Copyright Statement

The authors confirm that they, and/or their company or organization, hold copyright on all of the original material included in this paper. The authors also confirm that they have obtained permission, from the copyright holder of any third party material included in this paper, to publish it as part of their paper. The authors confirm that they give permission, or have obtained permission from the copyright holder of this paper, for the publication and distribution of this paper as part of the ICAS2010 proceedings or as individual off-prints from the proceedings.